ARTICLE

Check for updates

Abrupt change in tropical Pacific climate mean state during the Little Ice Age

Ana Prohaska [1,2,8 ✉], Alistair W. R. Seddon [3,4], Bernd Meese[5], Katherine J. Willis[1,9], John C. H. Chiang [6] & Dirk Sachse [7]

The mean state of the tropical Pacific ocean-atmosphere climate, in particular its east-west asymmetry, has profound consequences for regional climates and for the El Niño/Southern Oscillation variability. Here we present a new high-resolution paleohydrological record using the stable-hydrogen-isotopic composition of terrestrial-lipid biomarkers (δD_{wax}) from a 1,400-year-old lake sedimentary sequence from northern Philippines. Results show a dramatic and abrupt increase in δD_{wax} values around 1630 AD with sustained high values until around 1900 AD. We interpret this change as a shift to significantly drier conditions in the western tropical Pacific during the second half of the Little Ice Age as a result of a change in tropical Pacific mean state tied to zonal sea surface temperature (SST) gradients. Our findings highlight the prominent role of abrupt shifts in zonal SST gradients on multidecadal to multicentennial timescales in shaping the tropical Pacific hydrology of the last millennium, and demonstrate that a marked transition in the tropical Pacific mean state can occur within a period of a few decades.

[1] Department of Zoology, University of Oxford, South Parks Road, Oxford, UK. [2] Department of Zoology, University of Cambridge, Downing St, Cambridge, UK. [3] Department of Biological Sciences, University of Bergen, Bergen, Norway. [4] Bjerknes Centre for Climate Research, University of Bergen, Bergen, Norway. [5] Fraunhofer Institute for Manufacturing Engineering and Automation, Stuttgart, Germany. [6] Department of Geography, University of California Berkeley, Berkeley, CA, USA. [7] Helmholtz Centre Potsdam, GFZ German Research Center for Geosciences, Section 4.6: Geomorphology, Potsdam, Germany. [8] Present address: Globe Institute, University of Copenhagen, Copenhagen, Denmark. [9] Present address: Department of Biology, University of Oxford, South Parks Road, Oxford, UK. ✉email: ana.prohaska@sund.ku.dk

A noticeable feature of the equatorial Pacific climate is its east-west asymmetry, with warmer ocean surface conditions to the west that supports atmospheric deep convection, and a colder east. Easterlies converge near the equator and drive surface waters to the west, deepening the thermocline to the west and shoaling it to the east; this allows equatorial upwelling to bring cooler waters on the eastern side. This asymmetry periodically breaks down in the modern-day climate, leading to transient El Niño conditions[1,2]. Persistent changes to this asymmetry that resemble the pattern of ENSO occurred in past climates, leading to the so-called 'permanent El Niño-like' conditions. While the surface climate pattern of these changes may resemble El Nino, they occur on longer timescales and through mechanisms that differ from the interannual case[3]. Marked "permanent El Niño-like" conditions were thought to occur in the Pliocene[4,5], and they have also been proposed to occur at various points in the Quaternary[6–9].

Understanding past mean changes to the east-west asymmetry is directly relevant to understanding tropical Pacific mean state changes under future warming[10]. Virtually all climate models project a pronounced warming in the eastern equatorial Pacific relative to the western equatorial Pacific. However, these projections fly against recently observed trends that show the **opposite** to have occurred during the last decades, suggesting that the model projections may be in error[10]. This potential error has strong implications for future regional projections of climate. Like interannual El Niño, multidecadal to multicentennial changes in sea surface temperatures (SST) in the tropical Pacific that mirror the ENSO pattern can lead to changes to regional climates throughout the globe mediated through atmospheric teleconnections. Paleoproxy information that documents changes to the tropical Pacific mean climate, in particular its east-west asymmetry, can provide a valuable perspective on this problem.

There is currently little consensus on the mean state of the Tropical Pacific during the Little Ice Age (LIA). SST reconstructions indicate relative warming in the eastern[11–13] and cooling in the western equatorial Pacific[14,15], suggesting a weak zonal gradient. In contrast, the majority of hydrological records suggest wetter conditions in the western tropical Pacific[16–20], and drier conditions in the central[21] and the eastern equatorial Pacific[22,23] during the LIA, consistent with a strong zonal SST gradient phase during this time. However, a number of records are not consistent with this hydrological trend, either indicating drier (wetter) conditions in the western (eastern) equatorial Pacific during the LIA[24,25], or showing no apparent trend[26].

This apparent discrepancy could be explained by other potential drivers of precipitation changes in the tropical Pacific, namely the Intertropical Convergence Zone (ITCZ) and East Asian Summer Monsoon (EASM) and Australian Summer Monsoon (ASM)[22,27]. Presently, it is difficult to differentiate the contribution of the different drivers to shaping the observed paleohydrological patterns during the LIA, because a sufficiently distributed set of paleo proxies that are able to differentiate between these drivers is currently lacking. However, one feature of all of these other drivers is that they are associated with warm-season **convective** rainfall. A proxy that primarily measures autumn-time orographic rainfall—as we will show for our proxy —would not be as influenced by these various drivers, and thus the climatic interpretation would be less ambiguous.

Here we report a new rainfall record, based on leaf-wax hydrogen isotope data (expressed as δD_{wax} values) from a 1,400-year-old sedimentary sequence from Bulusan Lake (N 12°45′, E 124°6′) in northeastern Philippines (Figs. 1 and 2). The region is a member of a recently identified global network of "Autumn Monsoon precipitation" regions[28]. Autumn monsoon regions occur on the eastern coast of land masses when trade winds

impinge on orography and the temperature is still sufficiently warm to support moist convection. Peak rainfall occurs when these regions are poleward of the ITCZ, and thus embedded in easterly low-level trades, usually between October and February at our site (Supplementary Fig. 1a). While the western North Pacific monsoon also operates over this region, its contribution to the annual rainfall amount is smaller. Additionally, typhoons are a source of episodic precipitation, and can potentially account for up to 30% of northeastern Philippines rainfall in exceptional years[29]. ENSO is the main driver of interannual rainfall variability at Bulusan, resulting in reduced (increased) precipitation during El Niño (La Niña) years (Supplementary Fig. 1b). Consequently, a rainfall record from Bulusan is highly suitable to provide insights into the mean changes to the east-west asymmetry of the Tropical Pacific climate system during the last millennium.

We show that a dramatic and abrupt rise in δD_{wax} values occurred around 1630 AD and persisted until roughly 1900 AD. This shift is interpreted as a movement towards substantially drier conditions in the western tropical Pacific during the latter part of the Little Ice Age, due to changes in the mean state of the tropical Pacific associated with zonal sea surface temperature gradients. Our results reveal a major influence of multidecadal to multicentennial changes of zonal SST gradients on the hydrology of the tropical Pacific over the past millennium. We also show that pronounced changes in the mean state of the tropical Pacific can transpire within a span of a few decades, a behavior that existing fully coupled climate models fail to replicate.

Results

Changes of δD_{wax} in the Bulusan core. The top 300 cm from two overlapping sediment cores (BUL1 and BUL2) collected from Bulusan Lake provide a continuous, undisturbed sedimentary sequence spanning the last 1400 years (Fig. 2d and Supplementary Fig. 2) (see Methods). An independent and robust age-depth model (Fig. 2c) has been established using 10 AMS[14]C dates (Supplementary Table 1 and Supplementary Note 1). Bulusan sediments contain abundant terrestrial-lipid biomarkers, specifically the n-alkanes with 27, 29, and 31 carbon atoms (nC_{27-31}) over this time period. We report D/H isotope ratios of those n-alkanes (expressed as δ^2H or δD values), as well as an independent record of fossil pollen abundance from the same sedimentary sequence to ensure adequate identification of biomarker sources[30] (Fig. 3) (see Methods).

The nC_{27-31} alkanes are a major component of the leaf waxes of higher terrestrial plants[31]. δD values of these alkanes (δD_{wax}) in the surface sediments of smaller lakes fed by precipitation and groundwater, such as Bulusan Lake, are significantly correlated with local rainfall δD values, offset by a biosynthetic fractionation[32]. δD_{wax} values can be additionally affected by evaporative deuterium enrichment of leaf water due to increased evapotranspiration under low atmospheric humidity[32,33]. At Bulusan, where the relative humidity is high year-round, leaf water deuterium enrichment is expected to be minimal[33], and therefore δD_{wax} at the site should faithfully record changes in δD values of precipitation (δD_{precip}).

δD values of the three abundant terrestrial-lipid biomarkers, nC_{27-31}, are highly correlated in the Bulusan core, with a coefficient of determination (r) ranging between 0.69 and 0.81 ($p < 10^{-6}$; Supplementary Fig. 3 and Supplementary Note 2), confirming a common origin of these alkanes. The average chain length of n-alkanes between nC_{25} and nC_{33} is stable throughout the record up until the 19th century when there is a slight decrease, possibly caused by the changes in the composition of surrounding vegetation due to increasing human activities in the area[34] (Supplementary Fig. 4 and Supplementary Note 3). Fossil
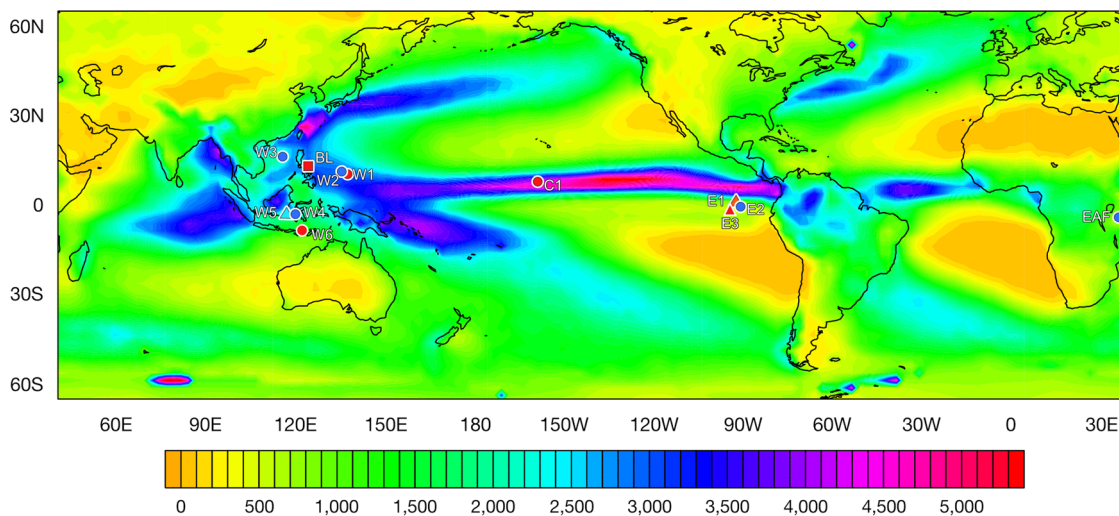
Fig. 1 Map of mean annual precipitation in the tropical Pacific showing the location of our study site, Bulusan Lake, and the locations of other hydrological and sea surface temperature records. In the western Pacific, Bulusan Lake (BL), Clear Lake (W1)[25], and Spooky Lake (W2)[21] in Palau Island, Dongdao Island (W3)[19], Makassar Strait (W4[16], W5[14,15]), and Liang Luar (W6)[51]. In the central Pacific, Washington Island (C1)[21], and in the eastern Pacific, El Junco Lake (E1)[11], Poza de la Diablas (E2)[24], and ocean multicore near Española Island (E3)[13] in the Galapagos Islands. Overall wetter and drier conditions during the Little Ice Age, derived from the mapped hydrological records (circles), are depicted in blue and red, respectively. Relevant sea surface temperature records (triangles), with overall warmer and cooler conditions during the Little Ice Age, are depicted in red and light blue, respectively. The band of heavy precipitation indicates the ITCZ. Modified figure from ref. [95].

pollen from the same sedimentary sequence reveals that the plant assemblages surrounding the lake during the last 1,400 years contained only a small fraction of grasses and sedges (C4 plants) (Fig. 3) and were dominated by trees and shrubs (Supplementary Note 4), the likely source of the nC_{27-31} alkanes[35]. The percentage of grass pollen remained stable between 0–5% throughout the record, indicating that there was no major change in the proportion of C_4 to C_3 plants, and rules out the possibility that vegetation changes have significantly affected δD_{wax} values[32]. However, the nC_{27} alkane (average relative abundance of 20%) in the record shows higher variability in comparison to nC_{29} (average relative abundance of 35%) and nC_{31} (average relative abundance of 45%) indicating more variable sources (Fig. 3, Supplementary Fig. 4, and Supplementary Note 5). Furthermore, previous studies have suggested that nC_{31} is a major constituent of grasses and herbs[36] in addition to trees[35], which may at least partly explain its reduced variance compared to nC_{29}. While δD_{wax} values of all three alkanes show the same pattern, we focus our interpretation on the nC_{29} alkane in order to minimize the potential distortion of the precipitation signal due to variability in alkane sources and deuterium enrichment differences between C_3 and C_4 plants.

δD values of nC_{29} varied by up to 45‰ during the study period indicating significant hydrological changes at Bulusan Lake over the last 1400 years (Fig. 3). Relatively low and stable δD_{wax} values occurred during AD 600–1600, followed by a distinct and abrupt increase in δD values at AD 1630 ± 35 (i.e., 20‰ within a period of a few decades, see Supplementary Table 2b, Supplementary Fig. 5, and Supplementary Note 6). These high δD_{wax} values persisted until ~AD 1900 ± 40 only to drop just as abruptly to their lowest values in the record over the last 100 years. Based on these elevated δD_{wax} values, we infer significantly drier conditions during the second half of the LIA (~AD 1630–1900), compared to the rest of the record.

Drivers of precipitation δD values at Bulusan. We use a range of instrumental datasets and global circulation model outputs to identify drivers of δD_{wax} (and therefore δD_{precip}) variations at

Bulusan, using the interannual variability to isolate enriched and depleted years. First, we use an isotope-enabled general circulation model (isoGSM2; see Methods) to understand the large-scale drivers of δD_{precip} values in the northeastern Philippines. Since the northeastern Philippines is spatially too limited for the rainfall to be adequately resolved in isoGSM2, we analyze instead the δD of precipitable water (hereafter δD_{pw}) for the isoGSM2 grid-point closest to that region (N 13°, E 124°); variations in δD_{pw} are found to closely match variations in the δD of station rainfall measured over that region (Supplementary Fig. 6 and Supplementary Table 3). We generate an interannual index of amount-weighted δD_{pw} (using July and the following June as the start and end months), and compare years with enriched δD_{pw} with depleted years (Fig. 4a). There is a clear El Niño influence for enriched years—the 1982–83, 1997–98, and 2015–16 El Niños stand out (Fig. 4a), and moreover the amount-weighted δD_{pw} index is correlated with an interannual index of ENSO (Nino3.4 averaged over the peak months of October-February, Fig. 5a) at $r = 0.75$ ($p < 0.001$; Fig. 4b). Years with more positive δD_{pw} values are drier over the northern Philippines during the autumn and winter rainfall months (October-February), because of reduced moisture flux from the northeasterly trades impinging on the northeastern Philippines (Fig. 4c, d). SST and rainfall changes associated with enriched relative to depleted δD_{pw} years (Fig. 4e) shows warming SST in the eastern equatorial Pacific and slight cooling over the western equatorial Pacific indicative of a weak zonal SST gradient, and commensurate changes to rainfall.

To further assess the influence of ENSO on δD_{pw} at Bulusan, we composite δD_{pw} of El Niño and La Niña years over the Bulusan gridpoint (N 13°, E 124°) and find that precipitable water is heavier (lighter) during El Niño (La Niña) years compared to neutral ENSO years, in particular over the autumn and winter months (Fig. 5b). Despite being highly negative and a mismatch in absolute values, as they are averaged for the entire atmospheric column of water vapor, the relative change between El Niño and La Niña years in modeled δD_{pw} values of about 11‰ is consistent with surface water observations[37]. Regionally, precipitable water is isotopically enriched over the western Tropical Pacific and
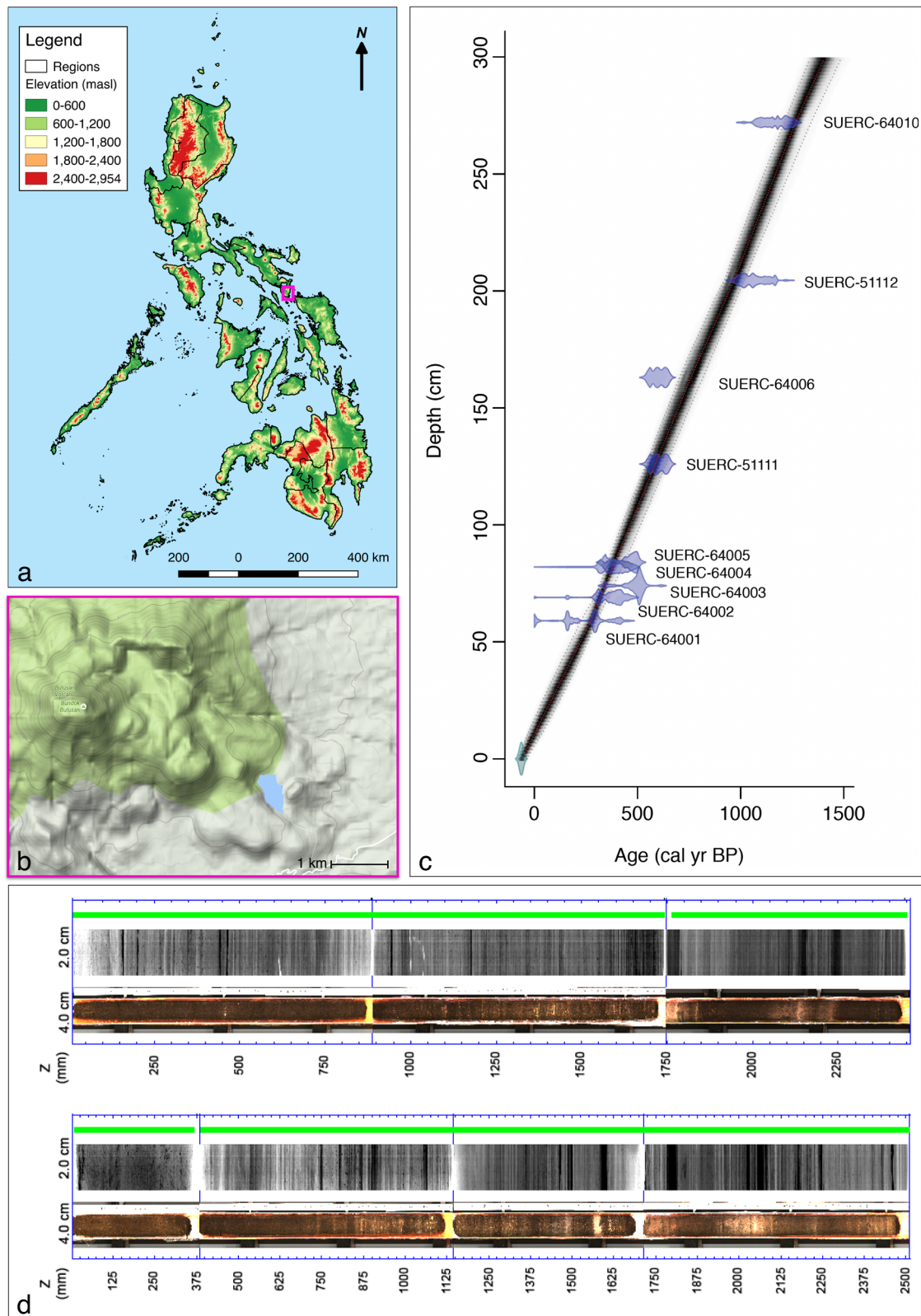
Maritime continent for El Niño years relative to La Niña years (Supplementary Fig. 7), accompanying the El Niño-driven reduction to rainfall over those regions. The two are causally related: El Niño reduces deep convection over the western tropical Pacific, and since convection depletes the isotopic composition of water vapor, water vapor in this region becomes isotopically enriched (Supplementary Fig. 7).

Similarly, differences in precipitation amount at Bulusan occur during the autumn and winter months between El Niño and La Niña years. Rainfall data from the Climate Research Unit TS version 4.03[38] dataset for the gridpoint nearest Bulusan (N 12°45′, E 124°15′) (see Methods) show that La Niña years have more precipitation than neutral ENSO years, and El Niño years have less (Fig. 5c). A similar relationship for precipitation and δD_{precip}

Fig. 2 Geographical and sedimentological features of the Bulusan site. a Topographic map of the Philippines showing the location of the Bulusan site. Data from PhilGIS[96], the map generated in QGIS version 2.14.3[97]. **b** Map showing Bulusan Lake (blue) within its larger landscape, with Mt Bulusan volcano in the west (green)[98]. **c** Age-depth model for the Bulusan sediment sequence, constructed with *Bacon* version 2.2[87,88] in R version 3.2.4[99]. Probability distributions for the radiocarbon dates are shown in blue. The top of the sediment sequence is assigned the year the cores were collected. The shaded areas represent the 1σ probability age ranges by interpolating between AMS[14]C age control points. The red dashed line represents the age-depth calibration used in further analysis. SUERC-64011 is not shown here as it lies below the analysed section. **d** Optical and radiograph profiles of the Bulusan sediments, generated in ItraxPlot program[100]. The radiograph images depict the level of organic content, with higher values shown as lighter bands. The green line represents the validation of the measurement quality along the cores. For more details on the physical and chemical characterization of Bulusan cores, see Supplementary Note 8.
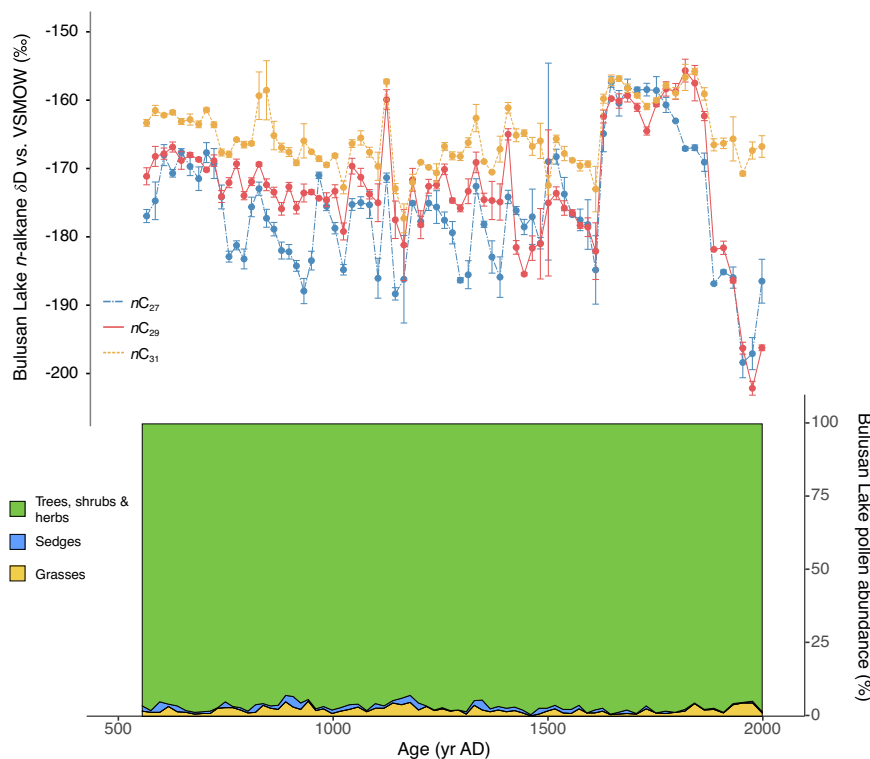

Fig. 3 Paleorecords from the Bulusan Lake. A record of H/D isotope ratio measurements of leaf-wax alkanes (nC_{27-31}), expressed as δD values with error bars of 1 standard deviation, and a record of fossil pollen abundance expressed as the percentage of grasses (Poaceae) and sedges (Cyperaceae), representing C4 plants, vs. other terrestrial plant taxa (trees, shrubs, and herbs), representing predominately C3 plants. Data plotted with *ggplot2* package[101] in R version 3.2.4[99].

can be observed in the Global Network of Isotopes in Precipitation (GNIP) data (Supplementary Fig. 8 and Supplementary Note 7), where the major difference between 1997 and 1998 is during the autumn and winter.

Our results demonstrate that δD_{pw} (and therefore also δD_{wax}) values are isotopically enriched, and rainfall is reduced, during El Niño years (weak zonal gradient) relative to La Niña years. The bulk of the rainfall changes occur during the autumn and winter months (October–February). This relationship to ENSO allows us to use Bulusan δD_{wax} to monitor past changes in the east-west asymmetry of the equatorial Pacific climate.

Discussion
Based on our analysis above, the distinct and abrupt increase in nC_{27-31} alkane δD values in the Bulusan paleorecord between ~AD 1630–1900 suggests an abrupt shift in the hydroclimate of the western tropical Pacific during the late LIA towards significantly drier conditions. Since the lowland tropics are characterized by low-temperature variability during the Holocene[26,39], the 'temperature effect' on the isotopic composition of precipitation in

these regions should be negligible[27] and is therefore not normally included in the interpretation of the δD changes in the paleorecords from the tropical Pacific from this time period.

While several paleohydrological records from the region have had changes in their isotopic signatures linked to shifts in the geographic position and extent of ITCZ[22,27], our isoGSM2 analysis confirms that at Bulusan δD_{precip} is primarily an autumn-time rainfall proxy[28], with ITCZ as a secondary contributor to variability in the record through its influence on summer precipitation. Specifically, our results indicate that ENSO is the key driver of present-day precipitation δD variations at Bulusan, as the decrease in convective activity over the western tropical Pacific during El Niño years leads to an enrichment of water vapor in the region (Supplementary Fig. 7). Furthermore, while previous interpretations of changes in precipitation stable isotopes in the region have focused on precipitation amount, our findings are supported by several recent studies which have suggested that ENSO can directly influence precipitation stable isotopic values on an interannual scale via alterations in the strength of convective activity across the tropics (e.g., refs. [40–42]). Additionally, a number of studies have demonstrated a mismatch
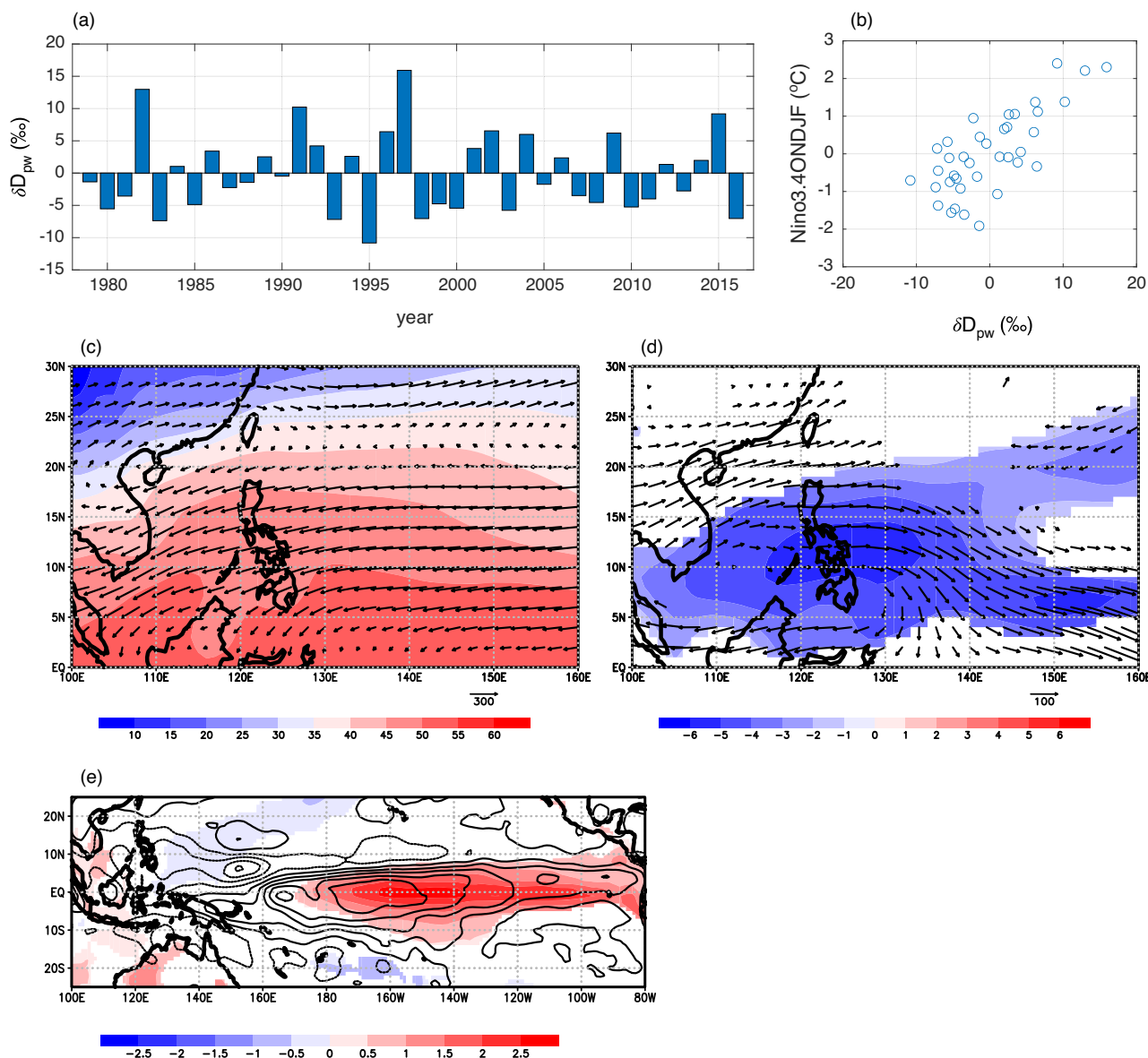
Fig. 4 Examination of δD values of precipitable water (δD$_{pw}$) of enriched vs. depleted years using isoGSM2 output. a Time Series of the amount-averaged δD$_{pw}$ over Bulusan, and correlation. δD at the gridpoint closest to Bulusan was amount-averaged from the preceding July through the following June. The mean (−151.23 per mil) was subtracted and the time series detrended prior to plotting. Years with high δD$_{pw}$ are enriched. **b** Scatterplot between the amount-weighted δD$_{pw}$ with an interannual index of ENSO (Nino3.4 averaged over the peak months of October-February). The two time series are correlated at $r = 0.75$ ($p < 0.001$). **c** Climatological vertically-integrated moisture flux during the northern Philippines wet months of October-February (vectors; reference vector is 300 (g kg^{-1}).(m s^{-1})), and the October-February precipitable water (shaded; units are kg m^{-2}). **d** Difference in the vertically-integrated moisture flux (vectors; reference vectors is 100 (g kg^{-1}).(m s^{-1})) and precipitable water (shaded; units are kg m^{-1}) averaged over October-February, enriched minus depleted years; the eight most enriched years in (**a**) are used for the enriched composite; similarly for depleted years. The precipitable water field is shaded only if the difference is significant at the 5% level, using a two-sided t-test; vectors are shown only if the difference for either the zonal or meridional flux is significant at the 5% level. For enriched years, there is reduced moisture flux by the northeasterly trades into the northern Philippines. **e** The difference in sea surface temperature (shaded, contour interval 0.5 K) and rainfall (contour interval 1.5 mm d^{-1}) averaged over October-February, for enriched minus depleted years. The sea surface temperature field is shaded only if the difference is significant at the 5% level, using a two-sided t-test.

between local precipitation and precipitation stable isotopes in the western tropical Pacific[43–46], instead implicating factors beyond the amount effect such as vapor transport history and the degree of vapor parcel distillation. Therefore, the variability in precipitation stable isotopes in the western tropical Pacific seem to be reflective of regional-scale atmospheric circulation rather than local rainfall amount.

Based on our modern climate system analysis showing ENSO having a dominant role in shaping interannual precipitation δD

dynamics at Bulusan, we propose a shift in the tropical Pacific mean state tied to the establishment of a weak zonal SST gradient in the tropical Pacific was responsible for the hydrological changes recorded during the second half of LIA in the Bulusan paleorecord. The reduction in the east-west asymmetry in the tropical Pacific mean state results in a reduced Walker circulation, leading to drier conditions over the western Pacific similar to what occurs during El Niño conditions today. Similarly, there would also be changes to the structure of convection in the
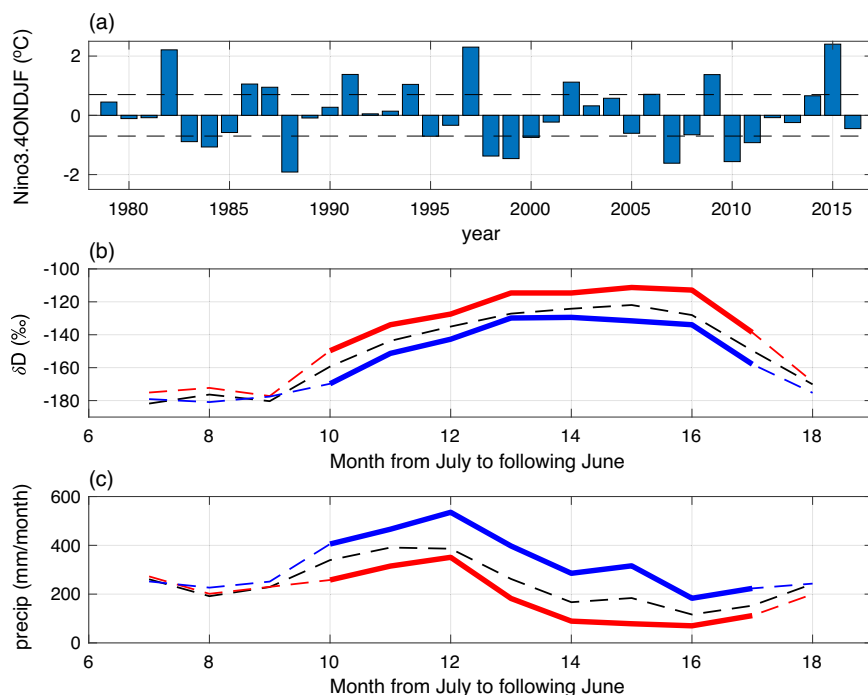
Fig. 5 Relationship between ENSO, precipitation, and precipitable water δD at Bulusan. a Nino3.4 averaged over October-February which we use as an interannual index of ENSO. We use +0.7 K as the threshold to identify El Niño years, and −0.7 K for La Niña years (horizontal dashed lines); the remainder of the years are neutral years. **b** δD of precipitable water for the El Niño (red), neutral (black), and La Niña (blue) composites at Bulusan. The thicker lines indicate the months when the difference between the El Niño and La Niña composites are significant at the 5% level using a two-sided t-test. Here, we use the isoGSM2 gridpoint nearest Bulusan Lake (N 13°, E 124°) for the δD field. **c** Precipitation for the El Niño (red), neutral (black), and La Niña (blue) composites at Bulusan. The thicker lines indicate the months when the difference between the El Niño and La Niña composites are significant at the 5% level using a two-sided t-test. Here, we use the CRU TSv4 rainfall gridpoint closest to Bulusan Lake, at N 12°45′, E 124°15′ (see Methods). Together, (**b**) and (**c**) shows that rainfall is reduced, and also isotopically heavier, for El Niño years compared to La Niña years.

tropical Pacific whereby the ITCZ of the northern tropical Pacific and the South Pacific Convergence Zone (SPCZ) collapses to a single ITCZ near the equator in the western and central equatorial Pacific, similar to what is seen during strong El Niño events today[47]. In the eastern Pacific, the northern ITCZ shifts equatorward as well. Since ENSO and the ITCZ are known to be strongly linked on interannual scales[48–50], we cannot exclude the potential for secondary influence by summer precipitation changes on the Bulusan record driven by the ITCZ dynamics, though our results suggest that changes in this climatic phenomenon is not something that Bulusan δD proxy predominately monitors.

Our results are supported by SST-based records from the tropical Pacific. The period of drier conditions at the Bulusan site corresponds to the period of relative warming in the eastern[11–13] and further cooling in the western equatorial Pacific[14,15] during the LIA, interpreted as a weak zonal SST gradient (Fig. 6). Importantly, the onset of cooling temperatures recorded in the Makassar Strait SST record[14,15] and of warming temperatures detected in the Galápagos multicore KNR195-5MC42C record[13] during the LIA period closely match the timing of the distinct increase in alkane δD values in the Bulusan paleorecord.

While several paleohydrological records from the region indicate the opposite situation, i.e., overall wetter conditions in the western Pacific[16–20], and overall drier conditions in the central[21] and the eastern Pacific[22,23] during the LIA, a number of these and other records indicate a change to reduced precipitation in the western Pacific (i.e., Makassar Strait[16]) and increased precipitation in the eastern Pacific (i.e., Poza de la Diablas[24]) between AD 1600 and 1900, which supports our interpretation (Fig. 7). Arguably, the strongest support from the tropical Pacific for our

results comes from the Liang Luar cave stalagmite δ18O record from Flores[51], which also suggests a marked shift from wetter to drier conditions at ~1600 AD. Data from ref. [52] from Eastern Africa offer additional support with strong climatic connections to ENSO today. The authors argued that the East African hydrological changes formed part of a larger tropics-wide climate change linked to warmer SSTs in the western Indian Ocean and cool SSTs in the eastern Indian Ocean and western Pacific warm pool, analogous to what is seen from teleconnections during El Niño events in present-day climate. The timing and nature of the East African hydrological changes match those seen in the Bulusan record, consistent with the onset of a weak zonal SST gradient.

A reduction in δD$_{wax}$ values in the Bulusan record around 1900 AD suggests a return to wetter conditions in the western tropical Pacific, indicative of a strong zonal SST gradient. Our results are in congruence with instrumental data which record a continued strengthening of the zonal SST gradient in recent decades, along with the sharp increase in the greenhouse gas (GHG) concentrations[53]. In contrast, state-of-the-art climate models predict that rising GHGs decrease the SST gradient across the tropical Pacific[41]. This striking mismatch between models and observational data has been recently explored by ref. [10], who attribute the erroneous model response to a well-known cold bias in the Pacific cold tongue as simulated by the coupled models. The Bulusan record provides a longer temporal perspective on this question, indicating that a trend of weak zonal SST gradient in the tropical Pacific may have started as early as early 1900s, though the low resolution of the age-depth model in the top section of the core hinders a more exact timing of the onset of this trend.
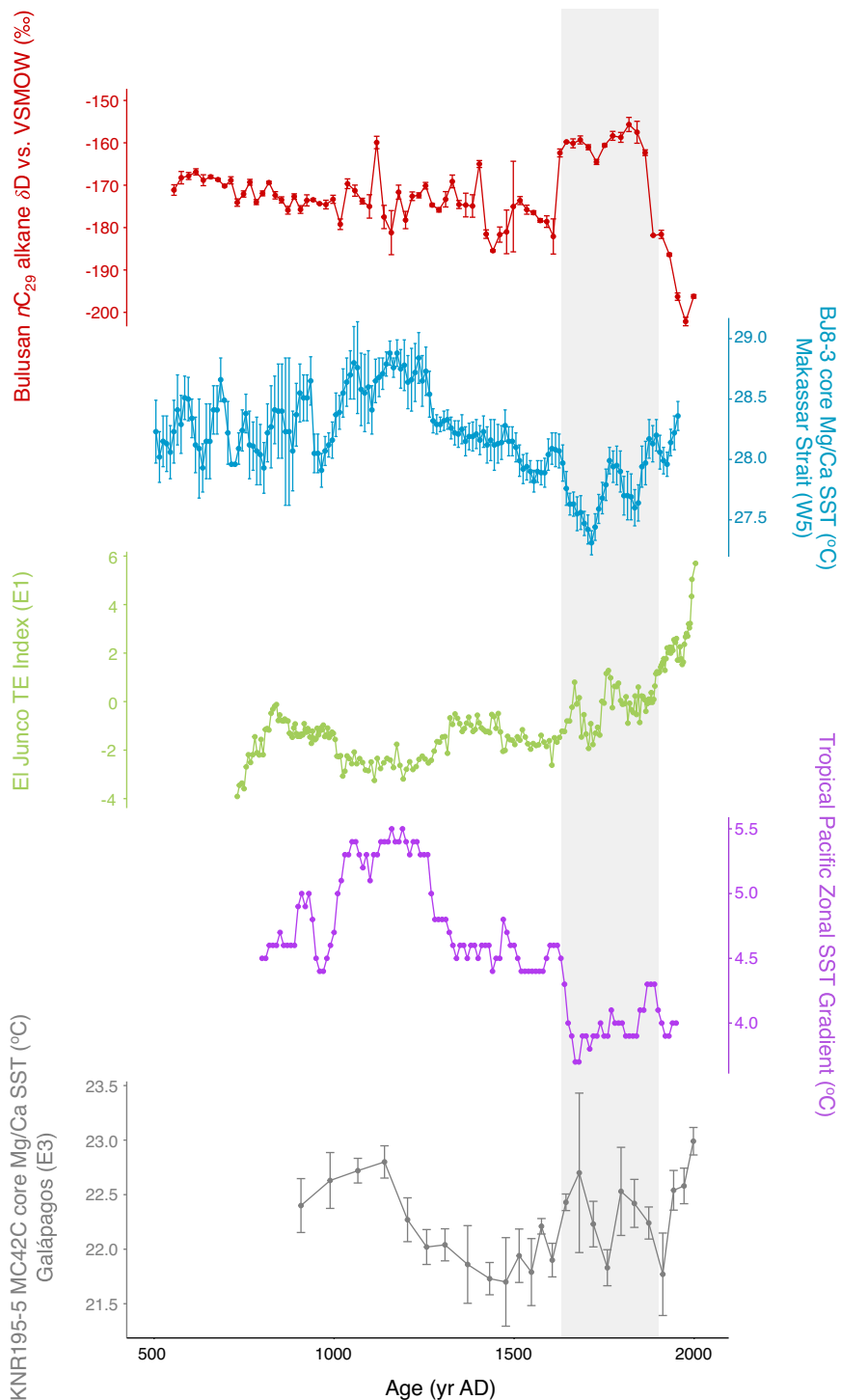
Fig. 6 Comparison of the Bulusan record (*n*C₂₉ alkane δD values) with regional SST records. In the western Pacific, Makassar Strait (W5, the error bars represent the standard error)[14,15,102], and in the eastern Pacific, El Junco Lake (E1)[11,12,103] and ocean multicore near Española Island (E3, the error bars represent 1 standard deviation)[13,104] in the Galápagos. Data plotted with ggplot2 package[101] in R version 3.2.4[99]. The gray strip denotes the period of significant pronounced change in the Bulusan record (~AD 1630–1900).

A remarkable feature of our record is the abrupt transition from low to high δD$_{wax}$ values between 1600 and 1650. While the resolution of the age-depth model precludes the estimation of the exact timing or rate of this transition in the Bulusan record (Supplementary Fig. 9), the results nevertheless emphasize that marked changes to the tropical Pacific mean state asymmetry can occur on decadal timescales. The shift from wetter to drier conditions at the Bulusan site happened over the period of only ~50

years, as did the subsequent return to wetter conditions ~270 years later. This finding is in accordance with SST-based zonal gradient reconstructions from the region. For instance, ref. [12] found that a change to a state of the weak zonal gradient of tropical Pacific SST at ~AD 1650 happened over the course of a few decades, very similar to the hydrological shifts recorded in the Bulusan record. Despite the increasing paleo-evidence, current fully coupled climate models do not reproduce such abrupt shifts
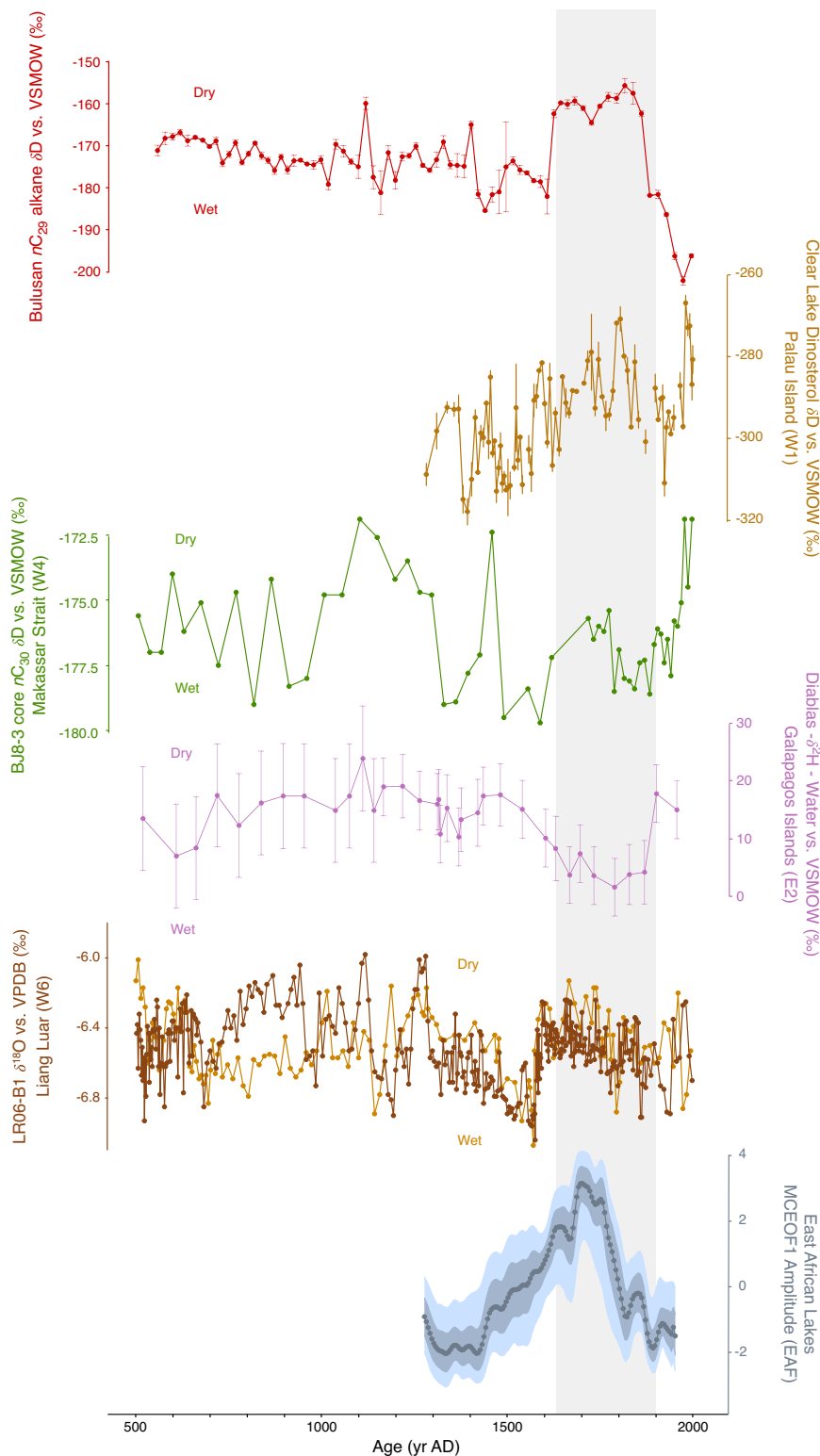
Fig. 7 Comparison of the Bulusan record (nC_{29} alkane δD values) with other paleohydrological records in the region. In the western Pacific, Clear Lake (W1, the error bars represent 1 standard deviation)[25], Makassar Strait (W4)[16], and Liang Luar (W6)[51,105], in the eastern Pacific, Poza de las Diablas (E2, the error bars represent 1 standard deviation)[24], and outside the tropical Pacific, the East Africa Lakes MCEOF record (EAF, 68 and 95% uncertainty bounds are shown in dark and light blue, respectively)[52]. Data plotted with ggplot2 package[101] in R version 3.2.4[99]. The gray strip denotes the period of significant change in the Bulusan record (~AD 1630–1900).

in tropical Pacific mean state, underlining potential limits in our mechanistic understanding.

Studies to date tend to describe the LIA in the tropical Pacific as having either an overall weak or strong zonal SST pattern, implying the entire period should be characterized by one mode or the other. However, the Bulusan record suggests, along with a number of other records in the tropical Pacific region[16,24,25,51], that there may have been a shift in the Pacific mean state dynamics approximately halfway through the LIA period. It is possible that the 1630–1900 AD event was caused by internal variability of the tropical Pacific climate system. However, while the relative roles of external forcing versus internal climate dynamics in generating (multi)decadal scale variability in the tropical Pacific have been widely discussed[54–57], an internally generated process driving (multi)decadal oscillations detected in palaeoclimate records has yet to be conclusively determined. In contrast, various means by which ENSO may influence the tropical Pacific mean state, and vice versa, have been previously described in refs. [58–65], highlighting how the relationship between the tropical Pacific mean state and ENSO variability is complex and interactive[13,66,67]. For instance, the influence of volcanic activity on ENSO has been widely demonstrated, with most observations (e.g., refs. [68,69]) and paleoclimate records (e.g., refs. [70–73]), as well as several modeling studies, suggesting that major tropical volcanic eruptions give rise to El Niño events[73–80]. Thus, one can imagine how the increased volcanic activity during LIA[81,82] may have amplified ENSO activity, and subsequently, caused or contributed to a shift to a weak zonal SST gradient in the tropical Pacific. While it is not possible to determine with existing data whether this shift was a result of internal variability or external forcing, we anticipate future studies focusing on this important question. For instance, high-resolution records of the subsurface thermal structure, a critical component of El Niño events[83], especially on longer timescales[84,85], would help to understand the patterns driving the SST gradient as well as the precipitation changes during this time period.

The prominent role of meridional shifts in the ITCZ in shaping tropical Pacific climate during the last millennium, and especially during the LIA, has been well established in previous studies[12,16,17,24,27]. Less certain is the nature and extent of the influence of (multi)decadal zonal ENSO-like shifts in the tropics during this time, and its interaction with meridional forcing from outside the tropics[51]. Our study directly addresses this knowledge gap. Overall, although the evidence presented here originates from a single site, our data, combined with other relevant paleohydrological and SST records from the region and modern observational and modeling data, make a strong case for a rapid change in tropical Pacific mean state linked to zonal SST gradients during the second half of the LIA. Our findings emphasize the prominent role of the tropical Pacific ocean-atmosphere mean climate, particularly its east-west asymmetry, in shaping precipitation patterns in the tropical Pacific over the past millennium through rapid, decadal changes in its mean state. Through atmospheric teleconnections, these changes could then be communicated globally to shift regional climates elsewhere, akin to what happens during an ENSO event today.

Methods

Study site and material collection. Bulusan Lake is a 0.28 km² oval-shaped lake located at 360 m.a.s.l., at the foot-slopes of Mount Bulusan volcano at the southeast end of the Bicol Volcanic Arc[86]. It consists of two basins: a small round basin, and a larger narrow basin, which are 12 and 24 m deep respectively. The two basins comprise a closed system fed primarily by precipitation and groundwater. The vegetation surrounding Bulusan Lake, and up the slope of Mt Bulusan, is classified as a Dipterocarp rainforest, i.e., aseasonal lowland tropical rainforest dominated by the Dipterocarpaceae tree family[34]. Two overlapping sedimentary sequences, 5.3 m BUL1 and 5.0 m BUL2, were collected as 1 m segments from the smaller basin with

a Livingstone Piston corer using an anchored platform in March 2013. The sediments were sealed in protective plastic containers and shipped to the University of Oxford where they have been stored at 5 ℃. Prior to subsampling, the cores were physically and chemically characterized (Supplementary Note 8).

Age-depth modeling. A robust age-model for the Bulusan sediments has been established with AMS[14]C dates (Supplementary Table 1) and the surface sediment set to 2013 (the year the core was collected). The radiocarbon analysis was done on identified terrestrial plant macrofossils (e.g., leaves, twigs) to avoid reservoir effects and minimize age uncertainty. AMS[14]C samples were measured at the NERC Radiocarbon Facility, East Kilbride. The age-depth modeling of the Bulusan core was performed using a Bayesian statistics approach to reconstruct accumulation histories for deposits with the Bacon 2.2 package in R[87,88] at 1 cm resolution and the IntCal13 radiocarbon calibration curve for the Northern Hemisphere[89], and model output estimates the age span per cm being between 4.5–6 years. For further details, see Supplementary Note 1.

Biomarker extraction, identification, and quantification. Sediment samples (n = 75) were sampled at the University of Oxford as a continuous series of 4 cm long slices (i.e., 2–6 g dry weight per sample) from a 300 cm long sequence, with each slice corresponding to a ~20-year interval. The samples were freeze-dried, and lipid biomarkers were extracted at the University of Potsdam with a dichloromethane (DCM): methanol mixture (9:1) at 100 ℃ and 103 bar using a Dionex accelerated solvent extraction system (ASE) 350. The extracts were separated into aliphatic and aromatic/alcohol/fatty acid fractions by solid phase extraction (SPE) in 8 ml glass columns filled with 2 g silica gel (0.040 to 0.063 mm mesh size) using hexane and DCM: methanol mixture (9:1) for elution, respectively, for a detailed description see the manual SPE extraction procedure in Rach et al.[90].

The n-alkanes (nC_{23-33} homologs) from the aliphatic fraction were identified and quantified at the University of Potsdam using a gas chromatograph (Agilent GC 7890-A) equipped with a mass selective detector-mass and a flame ionization detector (FID) (Agilent MS 5975-C) coupled via an electronic split interface. The MSD trace was employed for compound identification. The peak area from the FID chromatogram was used for compound quantification by calibrating against the peak area of the internal standard 5α-androstane. Sulfur and unsaturated hydrocarbons were removed from the aliphatic fraction by elution through a pipette column of activated copper powder and a pipette column of an activated mix of silver nitrate and silica gel, respectively, by applying a combination of hexane and dichloromethane (DCM). The resulting aliphatic fraction produced clean chromatograms and no unresolved complex mixture (UCM) was detected (except in Samples 1–6).

Compound-specific hydrogen isotope measurement of n-alkanes. Compound-specific hydrogen isotope ratios of the aliphatic fraction were measured at the University of Potsdam using a Thermo Fisher Delta-V-Plus Isotope Ratio Mass Spectrometer coupled to a Thermo Fisher TraceGC 1310 gas chromatograph. The samples were measured on a 50 m HP ultra 1 column with an inner diameter of 0.2 mm and a film thickness of 0.33 µm. The samples were measured with the following GC-temperature program: (i) temperature was held for 2 min at 40 ℃, (ii) temperature was increased to 256 ℃ at a rate of 4 ℃ per min, (iii) oven temperature was increased to 300 ℃ at 2 ℃ per min, and (iv) the final temperature was held for 45 min. The alkane standard mix was measured with a shorter program where the final temperature of 300 ℃ was held for 3 min only, as all standard peaks had eluted. The samples were measured in triplicates, with the exception of the top six samples which were measured in duplicates due to low compound concentrations.

A standard containing nC_{16} to nC_{30} alkanes with known δD values (mix A4, Arndt Schimmelmann, University of Indiana) was measured in duplicate at the beginning and the end of each sequence or after six sample injections, and then used for normalization of δD values to the Vienna Standard Mean Ocean Water (VSMOW) scale. The mean standard deviation of all measured samples for the nC_{27}, nC_{29}, and nC_{31} alkanes (n = 75) was about 1.6‰, 1.3‰, and 0.9‰, respectively. The H3+ factor was determined once a day and remained constant over the measurement period, indicating stable ion source conditions.

Isotope evaluation. Compounds with intensities below 800 mV (on mass 2) (i.e., nC_{23} and nC_{25}) were not used for evaluation, since this was outside of the linear range of the GC-IRMS system. In addition, an exclusively higher terrestrial plant origin of nC_{25} is difficult to assume because the alkane can be produced by aquatic plants such as Potamogeton. Therefore, for our interpretations we only used δD values of alkanes with 27, 29, and 31 carbon atoms (nC_{27-31}), which showed clean, baseline-separated peaks in all samples (except nC_{31} in Sample 2 which coeluted with an unidentified substance). The nC_{27-31} alkanes are the most widely used leaf-wax biomarkers and their hydrogen isotopic composition has been shown as a robust recorder of plant source water δD along extraordinarily steep climatic gradients[31].

Extraction and processing of fossil pollen. Sediment samples were extracted as a continuous series of 4 cm long 1 cm³ slices from the top 3.0 m of the composite

Bulusan core, with each slice corresponding to a ~20-year interval. Standardized protocols were employed for the extraction and processing of fossil pollen from the sediment samples[91]. 500 terrestrial pollen grains were counted in each sample (and identified to family or genus level where possible), and the relative abundance of grasses (Poaceae) and sedges (Cyperaceae) at each level was calculated as the proportion of Poaceae and Cyperaceae pollen in the total terrestrial pollen counts (expressed in percentages), at the same extent and resolution as the δD_{wax} records.

Modern rainfall data. We use the Climate Research Unit gridded Time Series version 4.03 dataset (CRU TSv4)[38] of monthly mean climatic quantities. Individual station rainfall data are combined and gridded onto a 0.5-degree horizontal grid using angular distance weighting. We use the gridpoint closest to Bulusan lake position (N 12°45′, E 125°15′), to represent the rainfall over that region. We also only use the time period overlapping with the isoGSM data, from 1979 to 2017.

Isotope-incorporated Global Spectral Model version 2 (IsoGSM2) simulation of precipitation isotopes. Output from an isotope-enabled general circulation model, the isoGSM version 2[92] between 1979 to 2017, is used in this study[30]. IsoGSM2 is based on a version of the Scripps Experimental Climate Prediction Center's global spectral model, but with the large-scale fields nudged towards the National Center for Environmental Prediction version 2 (NCEP2) reanalyzes[92,93]. Nudging is done for temperature, zonal and meridional winds only, and only for large (>1000 km) spatial scales. In this respect, the isoGSM2 simulation is similar to NCEP2, but with the addition of precipitation isotopes. The simulated precipitation isotopes have been shown to be realistic when compared to observations[94]; however, because of the relatively coarse horizontal resolution of isoGSM2 (T62, corresponding to 1.89 degrees at the equator), northeastern Philippines rainfall is not adequately resolved. In lieu of using precipitation isotopes from isoGSM2, we use the simulated δD of precipitable water (δD_{pw}) at the gridpoint closest to Bulusan Lake to assess changes to the δD of rainfall. The underlying assumption here is that changes to δD of rainfall reflect changes to the δD of vapor supplying the rainfall. We support this assumption by showing that changes in the simulated δD_{pw} compared favorably with observed δD measured by GNIP (see Supplementary Fig. 6 and Supplementary Note 9).

ENSO analysis. We derive an interannual index of ENSO by taking the average of sea surface temperature monthly anomalies over the Nino3.4 region (5S-5N, 170W-120W), and then averaging over the ENSO peak months of October through February; the index is subsequently referred to as Nino3.4ONDJF. To obtain the El Niño and La Niña composites for Fig. 5, we define years where Nino3.4ONDJF > 0.7 as El Niño years, and Nino3.4ONDJF <−0.7 as La Niña years.

Reporting summary. Further information on research design is available in the Nature Portfolio Reporting Summary linked to this article.

Data availability
All data needed to appraise the conclusions in the paper are shown in the Main Text and/or the Supplementary Information. The CRU TSv4 dataset is available at https://crudata.uea.ac.uk/cru/data/hrg, and monthly mean isoGSM2 model data, isotopic measurements, and composite pollen count data used in this study can be found at: https://doi.org/10.5880/GFZ.4.6.2020.007. The Nino3.4 index was taken from NOAA Physical Sciences Laboratory (NOAA PSL): https://psl.noaa.gov/gcos_wgsp/Timeseries/Nino34.

References
1. Bjerknes, J. A possible response of the atmospheric Hadley circulation to equatorial anomalies of ocean temperature. *Tellus* **18**, 820–829 (1966).
2. Bjerknes, J. Atmospheric teleconnections from the equatorial Pacific. *Mon. Weather Rev.* **97**, 163–172 (1969).
3. DiNezio, P., Clement, A. & Vecchi, G. Reconciling differing views of tropical Pacific climate change. *Eos, Transactions American Geophysical Union* **91**, 141–142 (2010).
4. Fedorov, A. V. et al. The Pliocene paradox (mechanisms for a permanent El Niño). *Science* **312**, 1485–1489 (2006).
5. Wara, M. W., Ravelo, A. C. & Delaney, M. L. Permanent El Niño-like conditions during the Pliocene warm period. *Science* **309**, 758–761 (2005).
6. Martin, L. et al. Southern oscillation signal in South American palaeoclimatic data of the last 7000 years. *Quat. Res.* **39**, 338–346 (1993).
7. Yamoah, K. A. A muted El Niño-like condition during late MIS 3. *Quat. Sci. Rev.* **254**, 106782 (2021).
8. Hällberg, P. L. et al. Seasonal aridity in the Indo-Pacific Warm Pool during the Late Glacial driven by El Niño-like conditions. *Clim. Past* **18**, 1655–1674 (2022).
9. Antinao, J. L. & McDonald, E. An enhanced role for the Tropical Pacific on the humid Pleistocene–Holocene transition in southwestern North America. *Quat. Sci. Rev.* **78**, 319–341 (2013).
10. Seager, R. et al. Strengthening tropical Pacific zonal sea surface temperature gradient consistent with rising greenhouse gases. *Nat. Clim. Chang.* **9**, 517–522 (2019).
11. Conroy, J. L. et al. Unprecedented recent warming of surface temperatures in the eastern tropical Pacific Ocean. *Nat. Geosci.* **2**, 46–50 (2009).
12. Conroy, J. L., Overpeck, J. T. & Cole, J. E. El Niño/Southern Oscillation and changes in the zonal gradient of tropical Pacific sea surface temperature over the last 1.2 ka. *PAGES news* **18**, 32–34 (2010).
13. Rustic, G. T., Koutavas, A., Marchitto, T. M. & Linsley, B. K. Dynamical excitation of the tropical Pacific Ocean and ENSO variability by Little Ice Age cooling. *Science* **350**, 1537–1541 (2015).
14. Newton, A., Thunell, R. & Stott, L. Climate and hydrographic variability in the Indo-Pacific Warm Pool during the last millennium. *Geophys. Res. Lett.* **33**, L19710 (2006).
15. Oppo, D. W., Rosenthal, Y. & Linsley, B. K. 2,000-year-long temperature and hydrology reconstructions from the Indo-Pacific warm pool. *Nature* **460**, 1113–1116 (2009).
16. Tierney, J. E., Oppo, D. W., Rosenthal, Y., Russell, J. M. & Linsley, B. K. Coordinated hydrological regimes in the Indo-Pacific region during the past two millennia. *Paleoceanography* **25**, PA1102 (2010).
17. Rodysill, J. R. et al. A paleolimnological record of rainfall and drought from East Java, Indonesia during the last 1,400 years. *J. Paleolimnol.* **47**, 125–139 (2012).
18. Zeng, Y. et al. The wet Little Ice Age recorded by sediments in Huguangyan Lake, tropical South China. *Quat. Int.* **263**, 55–62 (2012).
19. Yan, H. et al. South China Sea hydrological changes and Pacific Walker Circulation variations over the last millennium. *Nat. Commun.* **2**, 293 (2011).
20. Konecky, B. L. et al. Intensification of southwestern Indonesian rainfall over the past millennium. *Geophys. Res. Lett.* **40**, 386–391 (2013).
21. Sachs, J. P. et al. Southward movement of the Pacific intertropical convergence zone AD 1400–1850. *Nat. Geosci.* **2**, 519–525 (2009).
22. Moy, C. M., Seltzer, G. O., Rodbell, D. T. & Anderson, D. M. Variability of El Niño/Southern Oscillation activity at millennial timescales during the Holocene epoch. *Nature* **420**, 162–165 (2002).
23. Conroy, J. L. et al. Holocene changes in eastern tropical Pacific climate inferred from a Galápagos lake sediment record. *Quat. Sci. Rev.* **27**, 1166–1180 (2008).
24. Nelson, D. B. & Sachs, J. P. Galápagos hydroclimate of the Common Era from paired microalgal and mangrove biomarker 2H/1H values. *Proc. Natl Acad. Sci. USA* **113**, 3476–3481 (2016).
25. Richey, J. N. & Sachs, J. P. Precipitation changes in the western tropical Pacific over the past millennium. *Geology* **44**, 671–674 (2016).
26. Griffiths, M. L. et al. Younger Dryas–Holocene temperature and rainfall history of southern Indonesia from δ18O in speleothem calcite and fluid inclusions. *Earth Planet. Sci. Lett.* **295**, 30–36 (2010).
27. Yan, H. et al. Dynamics of the intertropical convergence zone over the western Pacific during the Little Ice Age. *Nat. Geosci.* **8**, 315–320 (2015).
28. Ramesh, N., Nicolas, Q. & Boos, W. R. The globally coherent pattern of autumn monsoon precipitation. *J. Clim.* **34**, 5687–5705 (2021).
29. Rodgers, E. B., Adler, R. F. & Pierce, H. F. Contribution of tropical cyclones to the North Pacific climatological rainfall as observed from satellites. *J. Appl. Meteorol.* **39**, 1658–1678 (2000).
30. Prohaska, A. et al. Paleosediment- and model-derived data used for the reconstruction of environmental conditions during the Holocene at the Bulusan Lake, Philippines. V. 1.1. *GFZ Data Services*. https://doi.org/10.5880/GFZ.4.6.2020.007 (2023).
31. Eglinton, G. & Hamilton, R. J. Leaf epicuticular waxes. *Science* **156**, 1322–1335 (1967).
32. Sachse, D. et al. Molecular paleohydrology: interpreting the hydrogen-isotopic composition of lipid biomarkers from photosynthesizing organisms. *Ann. Rev. Earth Planet. Sci.* **40**, 221–249 (2012).
33. Kahmen, A. et al. Leaf water deuterium enrichment shapes leaf wax n-alkane δD values of angiosperm plants II: observational evidence and global implications. *Geochim. Cosmochim. Acta* **111**, 50–63 (2013).
34. E. Abada Gatumbato, W. Carandang, N. Pampolina, N. A. Mallar, S. Narvadez. Final Report: Physical and Geopolitical Characteristics, Biological Resources, Socio-Cultural and Economics Conditions and Institutional Arrangements/Governance of the Bulusan Volcano Natural Park. *Resources, Environment and Economics Center for Studies Philippines* (2011).
35. Feakins, S. J. et al. Production of leaf wax n-alkanes across a tropical forest elevation transect. *Org. Geochem.* **100**, 89–100 (2016).
36. Schwark, L., Zink, K. & Lechterbeck, J. Reconstruction of postglacial to early Holocene vegetation history in terrestrial Central Europe via cuticular lipid biomarkers and pollen records from lake sediments. *Geology* **30**, 463 (2002).

37. Lee, J.-E. et al. Asian monsoon hydrometeorology from TES and SCIAMACHY water vapor isotope measurements and LMDZ simulations: Implications for speleothem climate record interpretation. *J. Geophys. Res. Atmos.* **117**, D15112 (2012).

38. Harris, I., Osborn, T. J., Jones, P. & Lister, D. Version 4 of the CRU TS monthly high-resolution gridded multivariate climate dataset. *Sci. Data* **7**, 109 (2020).

39. van Breukelen, M. R., Vonhof, H. B., Hellstrom, J. C., Wester, W. C. G. & Kroon, D. Fossil dripwater in stalagmites reveals Holocene temperature and rainfall variation in Amazonia. *Earth Planet. Sci. Lett.* **275**, 54–60 (2008).

40. Cai, Z. & Tian, L. Atmospheric controls on seasonal and interannual variations in the precipitation isotope in the East Asian Monsoon Region. *J. Clim.* **29**, 1339–1352 (2016).

41. Gao, J., He, Y., Masson-Delmotte, V. & Yao, T. ENSO effects on annual variations of summer precipitation stable isotopes in Lhasa, Southern Tibetan Plateau. *J. Clim.* **31**, 1173–1182 (2018).

42. Hurley, J. V., Vuille, M. & Hardy, D. R. On the interpretation of the ENSO signal embedded in the stable isotopic composition of Quelccaya Ice Cap, Peru. *J. Geophys. Res. Atmos.* **124**, 131–145 (2019).

43. Cobb, K. M., Adkins, J. F., Partin, J. W. & Clark, B. Regional-scale climate influences on temporal variations of rainwater and cave dripwater oxygen isotopes in northern Borneo. *Earth Planet. Sci. Lett.* **263**, 207–220 (2007).

44. Kurita, N., Ichiyanagi, K., Matsumoto, J., Yamanaka, M. D. & Ohata, T. The relationship between the isotopic content of precipitation and the precipitation amount in tropical regions. *J. Geochem. Explor.* **102**, 113–122 (2009).

45. Moerman, J. W. et al. Diurnal to interannual rainfall δ18O variations in northern Borneo driven by regional hydrology. *Earth Planet. Sci. Lett.* **369–370**, 108–119 (2013).

46. Conroy, J. L., Cobb, K. M. & Noone, D. Comparison of precipitation isotope variability across the tropical Pacific in observations and SWING2 model simulations. *J. Geophys. Res. Atmos.* **118**, 5867–5892 (2013).

47. Chiang, J. C. H. The tropics in paleoclimate. *Ann. Rev. Earth Planet. Sci.* **37**, 263–297 (2009).

48. Mamalakis, A. et al. Zonally contrasting shifts of the tropical rain belt in response to climate change. *Nat. Clim. Change* **11**, 1–9 (2021).

49. Cai, W. et al. Increasing frequency of extreme El Niño events due to greenhouse warming. *Nat. Clim. Change* **4**, 111–116 (2014).

50. Cai, W. et al. ENSO and greenhouse warming. *Nat. Clim. Change* **5**, 849–859 (2015).

51. Griffiths, M. L. et al. Western Pacific hydroclimate linked to global climate variability over the past two millennia. *Nat. Commun.* **7**, 11719 (2016).

52. Tierney, J. E., Smerdon, J. E., Anchukaitis, K. J. & Seager, R. Multidecadal variability in East African hydroclimate controlled by the Indian Ocean. *Nature* **493**, 389–392 (2013).

53. Coats, S. & Karnauskas, K. B. Are simulated and observed twentieth century tropical pacific sea surface temperature trends significant relative to internal variability?: tropical pacific SST trends in CGCMs. *Geophys. Res. Lett.* **44**, 9928–9937 (2017).

54. Henley, B. J. Pacific decadal variability: indices, patterns and tropical extratropical interactions. *Glob. Planet. Change* **155**, 42–55 (2017).

55. Newman, M., Compo, G. P. & Alexander, M. A. ENSO-forced variability of the Pacific Decadal Oscillation. *J. Clim.* **16**, 3853–3857 (2003).

56. Mann, M. E., Steinman, B. A. & Miller, S. K. Absence of internal multidecadal and interdecadal oscillations in climate model simulations. *Nat. Commun.* **11**, 49 (2020).

57. Mann, M. E., Steinman, B. A., Brouillette, D. J. & Miller, S. K. Multidecadal climate oscillations during the past millennium driven by volcanic forcing. *Science* **371**, 1014–1019 (2021).

58. Timmermann, A. A nonlinear mechanism for decadal El Niño amplitude changes. *Geophys. Res. Lett.* **29**, GL013369 (2002).

59. Timmermann, A. Decadal ENSO amplitude modulations: a nonlinear paradigm. *Glob. Planet. Change* **37**, 135–156 (2003).

60. Jin, F.-F. Strong El Niño events and nonlinear dynamical heating. *Geophysi. Res. Lett.* **30**, GL016356 (2003).

61. An, S.-I. & Jin, F.-F. Nonlinearity and asymmetry of ENSO. *J. Clim.* **17**, 2399–2412 (2004).

62. Liang, J., Yang, X.-Q. & Sun, D.-Z. The effect of ENSO events on the tropical Pacific mean climate: insights from an analytical model. *J. Clim.* **25**, 7590–7606 (2012).

63. Hayashi, M. & Jin, F. Subsurface nonlinear dynamical heating and ENSO asymmetry. *Geophys. Res. Lett.* **44**, GL075771 (2017).

64. Karnauskas, K. B., Smerdon, J. E., Seager, R. & González-Rouco, J. F. A Pacific centennial oscillation predicted by coupled GCMs. *J. Clim.* **25**, 5943–5961 (2012).

65. Samanta, D. et al. Coupled model biases breed spurious low-frequency variability in the tropical Pacific Ocean. *Geophys. Res. Lett.* **45**, GL079455 (2018).

66. Koutavas, A. & Joanides, S. El Niño-Southern Oscillation extrema in the Holocene and Last Glacial Maximum. *Paleoceanography* **27**, PA4208 (2012).

67. Sadekov, A. Y. et al. Palaeoclimate reconstructions reveal a strong link between El Niño-Southern Oscillation and Tropical Pacific mean state. *Nat. Commun.* **4**, 2692 (2013).

68. Sigl, M. et al. Timing and climate forcing of volcanic eruptions for the past 2,500 years. *Nature* **523**, 543–549 (2015).

69. Tung, K.-K. & Zhou, J. The Pacific's response to surface heating in 130 Yr of SST: La Niña–like or El Niño–like? *J. Atmos. Sci.* **67**, 2649–2657 (2010).

70. Brad Adams, J., Mann, M. E. & Ammann, C. M. Proxy evidence for an El Niño-like response to volcanic forcing. *Nature* **426**, 274–278 (2003).

71. McGregor, S., Timmermann, A. & Timm, O. A unified proxy for ENSO and PDO variability since 1650. *Clim. Past* **6**, 1–17 (2010).

72. Li, J. et al. El Niño modulations over the past seven centuries. *Nat. Clim. Chang.* **3**, 822–826 (2013).

73. Khodri, M. et al. Tropical explosive volcanic eruptions can trigger El Niño by cooling tropical Africa. *Nat. Commun.* **8**, 778 (2017).

74. Mann, M. E., Cane, M. A., Zebiak, S. E. & Clement, A. Volcanic and solar forcing of the tropical Pacific over the past 1000 Years. *J. Clim.* **18**, 447–456 (2005).

75. Ohba, M., Shiogama, H., Yokohata, T. & Watanabe, M. Impact of strong tropical volcanic eruptions on ENSO simulated in a coupled GCM. *J. Clim.* **26**, 5169–5182 (2013).

76. Maher, N., McGregor, S., England, M. H. & Gupta, A. S. Effects of volcanism on tropical variability. *Geophys. Res. Lett.* **42**, 6024–6033 (2015).

77. Stevenson, S., Otto-Bliesner, B., Fasullo, J. & Brady, E. 'El Niño like' hydroclimate responses to last millennium volcanic eruptions. *J. Clim.* **29**, 2907–2921 (2016).

78. Predybaylo, E., Stenchikov, G. L., Wittenberg, A. T. & Zeng, F. Impacts of a Pinatubo-size volcanic eruption on ENSO. *J. Geophys. Res. Atmos.* **122**, 925–947 (2017).

79. Liu, F. et al. Divergent El Niño responses to volcanic eruptions at different latitudes over the past millennium. *Clim. Dyn.* **50**, 3799–3812 (2018).

80. Zuo, M., Man, W., Zhou, T. & Guo, Z. Different impacts of northern, tropical, and southern volcanic eruptions on the tropical Pacific SST in the last millennium. *J. Clim.* **31**, 6729–6744 (2018).

81. Sigl, M. et al. Insights from Antarctica on volcanic forcing during the Common Era. *Nat. Clim. Chang.* **4**, 693–697 (2014).

82. Liu, J. et al. Centennial variations of the global monsoon precipitation in the last millennium: results from ECHO-G model. *J. Clim.* **22**, 2356–2371 (2009).

83. McPhaden, M.; Santoso, A.; Cai, W. in *El Niño Southern Oscillation in a Changing Climate* (eds McPhaden, M. J., Santoso, A. & Cai, W.) Ch. 1 (John Wiley and Sons, 2020).

84. DiNezio, P., Clement, A. & Vecchi, G. Reconciling differing views of tropical Pacific climate change, Eos Trans. *AGU* **91**, 141–142 (2010).

85. Dinezio, P. et al. The response of the Walker circulation to Last Glacial Maximum forcing: implications for detection in proxies. *Paleoceanography.* **26**, PA002083 (2011).

86. Delfin, F. G., Panem, C. C. & Defant, M. J. Eruptive history and petrochemistry of the Bulusan volcanic complex: implications for the hydrothermal system and volcanic hazards of Mt. Bulusan, Philippines. *Geothermics* **22**, 417–434 (1993).

87. Blaauw, M. & Andrés Christen, J. Flexible paleoclimate age-depth models using an autoregressive gamma process. *Bayesian Anal.* **6**, 457–474 (2011).

88. Blaauw, M. & Christen, J. A. Bacon 2.2. http://www.chrono.qub.ac.uk/blaauw/bacon.html (2015).

89. Reimer, P. J. et al. IntCal13 and Marine13 radiocarbon age calibration curves 0–50,000 years cal BP. *Radiocarbon* **55**, 1869–1887 (2013).

90. Rach, O., Hadeen, X. & Sachse, D. An automated solid phase extraction procedure for lipid biomarker purification and stable isotope analysis. *Org. Geochem.* **142**, 103995 (2020).

91. Bennett, K. D. & Willis, K. J. in *Tracking Environmental Change Using Lake Sediments. Developments in Paleoenvironmental Research* (eds Smol, J.P., Birks, H.J.B., Last, W.M., Bradley, R.S., Alverson, K.) Ch. 2 (Springer, 2001).

92. Yoshimura, K. Stable water isotopes in climatology, meteorology, and hydrology: a review. *J. Meteorol. Soc. Japan. Ser. II* **93**, 513–533 (2015).

93. Kanamitsu, M. et al. NCEP–DOE AMIP-II reanalysis (R-2). *Bull. Am. Meteorol. Soc.* **83**, 1631–1643 (2002).

94. Yoshimura, K., Kanamitsu, M., Noone, D. & Oki, T. Historical isotope simulation using reanalysis atmospheric data. *J. Geophys. Res.* **113**, D19108 (2008).

95. Wallace, J. M., Mitchell, T. P., Lau, A. K.-H. Legates/MSU precipitation climatology. http://research.jisao.washington.edu/legates_msu/ (1995).

96. PHILGIS. Philippine GIS Datasets. http://philgis.org/gis-data (2017).

97. Quantum GIS Development Team. Quantum GIS geographic information system. Open source geospatial foundation project. http://qgis.osgeo.org (2016).

98. SIO, NOAA, U.S.Navy, NGA, 348 GEBCO, Image Landsat, Data LDEO-Colombia, NSF. Google Earth Map [7.1.5.1557. Bulusan Lake, Philippines. 12° 26' 07.68" N, 123° 347 48' 29.53" E, Eye alt 2683.13 km]. (2016).

99. R Core Team. R: a language and environment for statistical computing. http://www.R-project.org/ (Foundation for Statistical Computing, 2013).

100. Rothwell, R. G. & Croudace, I. W. in *Micro-XRF Studies of Sediment Cores: Applications of a Non-destructive Tool for the Environmental Sciences* (eds Croudace, I. W. & Rothwell, R. G.) Ch. 26 (Springer, 2015).

101. Wickham, H. *ggplot2: Elegant Graphics for Data Analysis* (Springer Science & Business Media, 2009).

102. Oppo, D. W. et al. Makassar Strait 2,000 Year Foraminiferal SST and d18Osw Reconstructions. IGBP PAGES/World Data Center for Paleoclimatology. Data Contribution Series # 2009-089. NOAA/NCDC Paleoclimatology Program, Boulder CO, USA (2009).

103. Conroy, J. L. et al. El Junco Lake, Galápagos Diatom T/E Index Data. IGBP PAGES/World Data Center for Paleoclimatology. Data Contribution Series # 2009-017. NOAA/NCDC Paleoclimatology Program, Boulder CO, USA (2009).

104. Rustic, G. T., Koutavas, A., Marchitto, T. M. & Linsley, B. K. NOAA/WDS Paleoclimatology - Eastern Tropical Pacific 1,000 Year Foraminferal d18O and Mg/Ca SST. NOAA National Centers for Environmental Information. https://doi.org/10.25921/9ngn-ch10 (2009).

105. Griffiths, M. L. et al. NOAA/WDS Paleoclimatology - Liang Luar Cave, Indonesia 2,000 Year Speleothem Isotope and Geochemical Data. NOAA National Centers for Environmental Information. https://doi.org/10.25921/c0qn-4536 (2010).

Author contributions

A.P. initiated and designed the study, collected lake sediments, co-acquired financial support, carried out the data analysis and interpretation, and co-wrote the paper. A.W.R.S., J.C.H.C., and B.M. contributed to the data analysis and paper writing, and A.W.R.S. and J.C.H.C. were also involved in data interpretation. K.J.W. contributed to paper writing and acquired financial support. D.S. contributed to the study design, co-acquired financial support, co-interpreted the results, and co-wrote the paper.

Competing interests

The authors declare no competing interests.

Additional information

Supplementary information The online version contains supplementary material available at https://doi.org/10.1038/s43247-023-00882-7.

Correspondence and requests for materials should be addressed to Ana Prohaska.

Peer review information *Communications Earth & Environment* thanks the other, anonymous, reviewer(s) for their contribution to the peer review of this work. Primary Handling Editor: Joe Aslin.

Reprints and permission information is available at http://www.nature.com/reprints

Publisher's note Springer Nature remains neutral with regard to jurisdictional claims in published maps and institutional affiliations.